Supplementary Information (SI) for Inorganic Chemistry Frontiers.
This journal is © the Partner Organisations 2026

Supporting Information for

Rare-Earth Inverse Sandwich Compounds Supported by A Dianionic Five-Membered Aromatic Ligand

Huan Wang, ‡a Hao-Lan Zhang, ‡a Yan-Cong Chen,[b] Tao Shang,[a] Ming Liu,[a] Xiao-Han Peng,[a] Ying Liu,[a] Ming-Liang Tong,*b and Fu-Sheng Guo*a

‡Huan Wang and Hao-Lan Zhang contributed equally.

a. Institute of Fundamental and Frontier Sciences, University of Electronic Science and Technology of China, Xiyuan Avenue 2006, Chengdu 611731, China.
E-mail: guofush@hotmail.com

b. Key Laboratory of Bioinorganic and Synthetic Chemistry of the Ministry of Education, School of Chemistry, IGCME, GBRCE for Functional Molecular Engineering, Sun Yat-Sen University, Guangzhou 510006, China.
E-mail: tongml@mail.sysu.edu.cn

Contents

FTIR spectroscopy
Fourier-transform infrared (FTIR) spectra with a scan range of 4000–400 cm^{-1} were recorded inside an argon-filled glovebox using a Bruker Alpha II spectrometer equipped with a platinum ATR module.

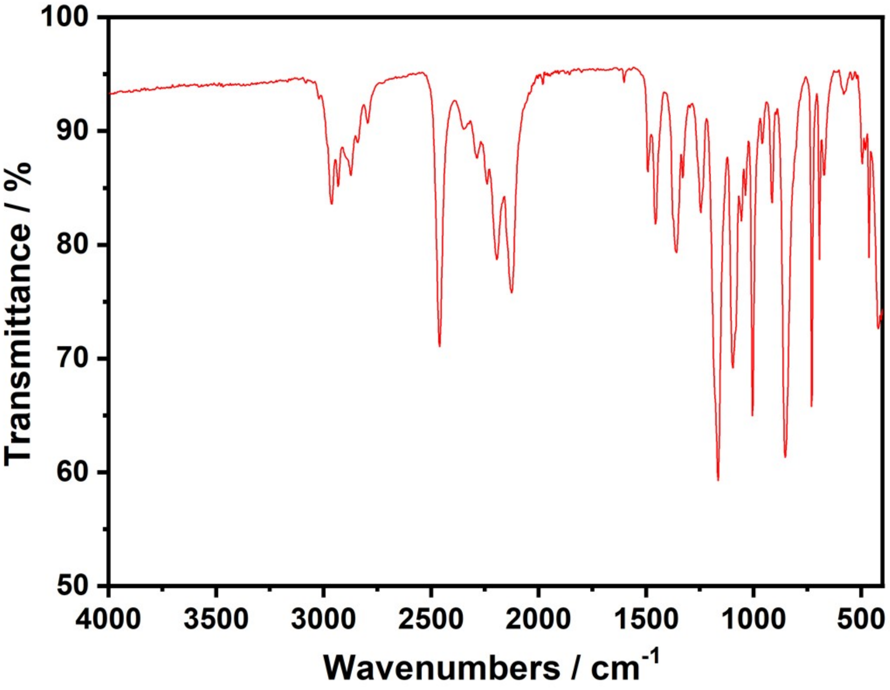

Fig. S1 FTIR spectrum of **1-Gd**.

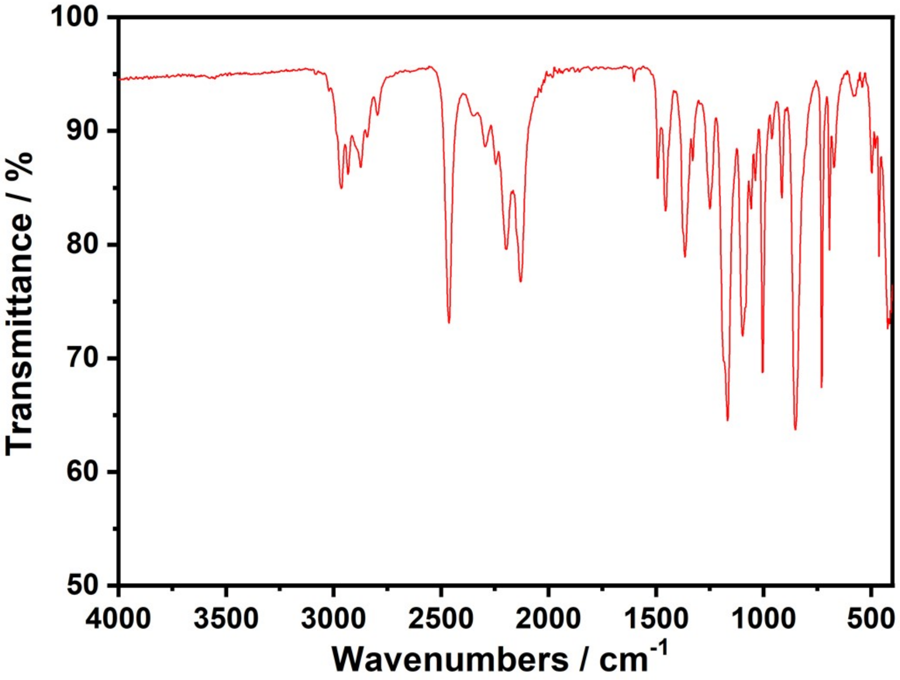

Fig. S2 FTIR spectrum of **1-Dy**.

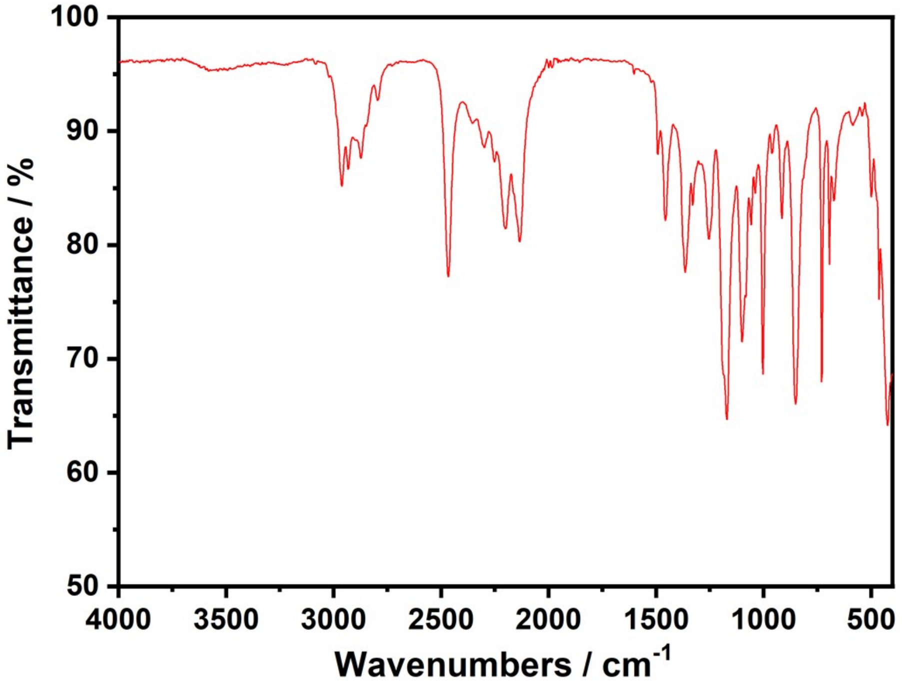

Fig.S3 FTIR spectrum of **1-Y**.

X-ray crystallography

X-ray diffraction data were collected for $[(\eta^5\text{-}(C_4B)^{Et4Me2N})RE_2(BH_4)_4(THF)_2]\cdot$toluene (RE = Gd, Dy, Y) on Bruker APEX-II CCD diffractometer, with all measurements conducted under specific protective conditions. The crystal was coated with perfluoropolyether oil, mounted on a crystal loop, and then flash-cooled under a stream of cold nitrogen gas generated by a cryogenic device. This setup maintained the crystal at a low temperature throughout the data collection process, during which unit cell determination and full structural data acquisition were performed at the specified temperature. Data collection and processing (cell refinement, data reduction and absorption) of the three compounds were performed using the program *APEX 5*. Structures were solved in Olex2 with SHELXT using intrinsic phasing and were refined with SHELXL using least squares minimisation.[1-3] Anisotropic thermal parameters were used for the non-hydrogen atoms and isotropic parameters for the hydrogen atoms. Hydrogen atoms were added geometrically and refined using a riding model. Deposition Number 2503310–2503312 contain the supplementary crystallographic data for this paper. These data can be obtained free of charge via the joint Cambridge Crystallographic Data Centre (CCDC) and Fachinformationszentrum Karlsruhe Access Structures service.

Table S1 Crystal data and structure refinement for **1-RE**.

Complex	**1-Gd**	**1-Dy**	**1-Y**
CCDC	2503310	2503311	2503312
Formula	$C_{29}H_{66}B_5Gd_2NO_2$	$C_{29}H_{66}B_5Dy_2NO_2$	$C_{29}H_{66}B_5Y_2NO_2$
FW	829.37	839.87	692.69
Crystal system	Monoclinic	Monoclinic	Monoclinic
Space group	*C2/c*	*C2/c*	*C2/c*
a/Å	19.4127(15)	19.2623(11)	19.2574(7)
b/Å	13.3323(11)	13.3685(7)	13.3690(5)
c/Å	15.7982(12)	15.8109(9)	15.8113(6)
α/°	90	90	90
β/°	114.987(2)	114.965(2)	114.9950(10)
γ/°	90	90	90
V/Å^3	3706.1(5)	3691.0(4)	3689.4(2)
Temperature/K	100.0	100.0	100.0
Z	4	4	4
ρ_{calc}/g cm^{-3}	1.486	1.511	1.247
Crystal size/mm^3	0.24×0.2×0.07	0.13×0.12×0.07	0.52×0.4×0.3
Radiation	Mo $K\alpha$ (λ = 0.71073)	Mo $K\alpha$ (λ = 0.71073)	Mo $K\alpha$ (λ = 0.71073
2θ range/°	3.832 to 61.192	4.148 to 61.02	3.838 to 61.16
Reflections collected	38989	47050	47231
Independent reflections	5670 [R_{int}=0.0559, R_{sigma}=0.0345]	5599 [R_{int}=0.0383, R_{sigma}=0.0213]	5640 [R_{int}=0.0621, R_{sigma}=0.0352]
Completeness/%	100.0	99.3	100.0
Data/restraints/parameters	5670/53/211	5599/67/201	5640/56/225
Goodness-of-fit on F^2	1.171	1.073	1.043
Final R indices [I>2σ(I)]	R_1= 0.0393 wR_2 = 0.0849	R_1= 0.0266 wR_2 = 0.0614	R_1= 0.0345 wR_2 = 0.0884
Final R indices (all data)	R_1 = 0.0447 wR_2 = 0.0870	R_1 = 0.0286 wR_2 = 0.0626	R_1 = 0.0462 wR_2 = 0.0942

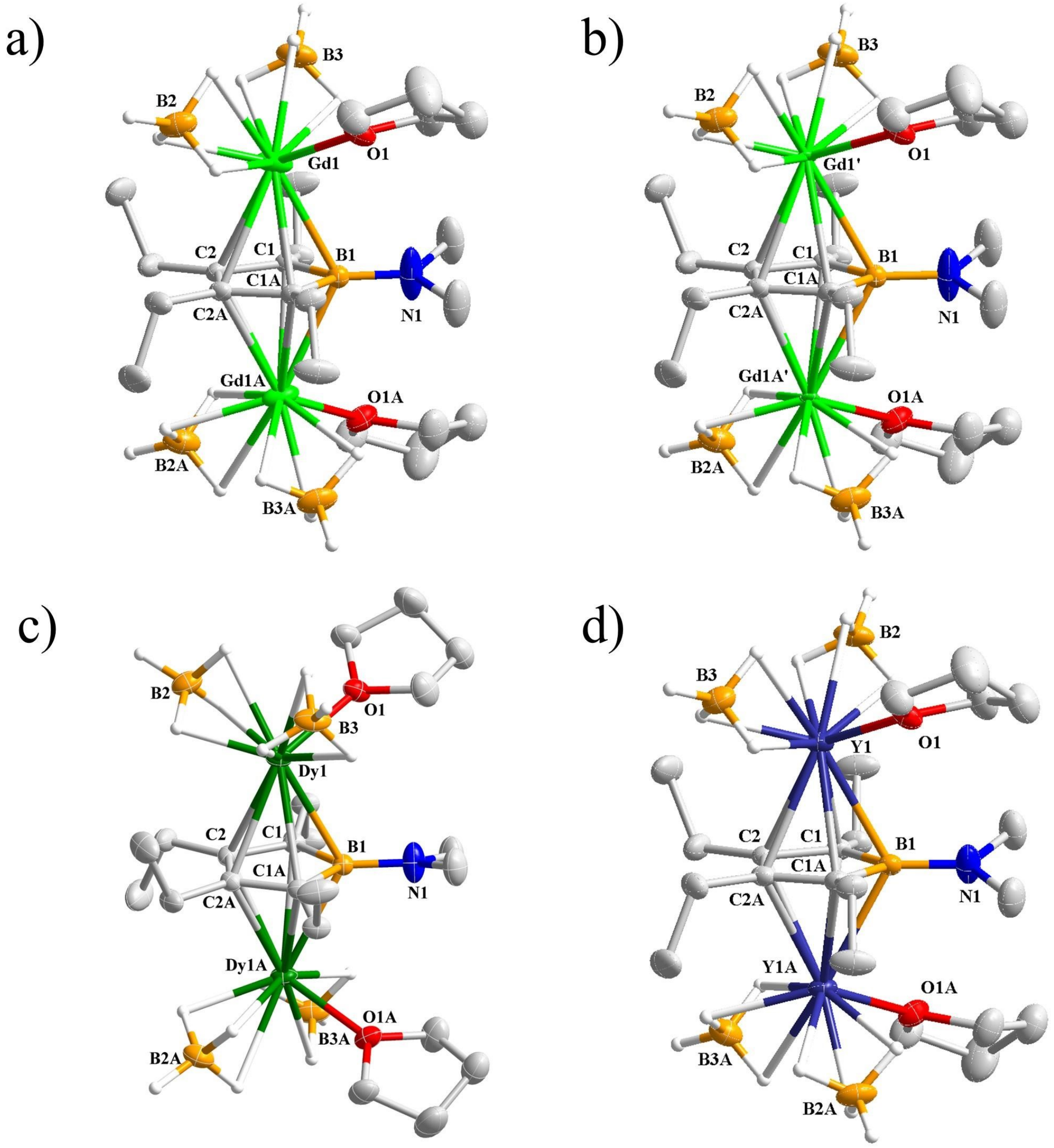

Fig. S4 Thermal ellipsoid representation (50% probability) of the molecular structures of $[(\eta^5\text{-}(C_4B)^{Et4Me2N})RE_2(BH_4)_4(THF)_2]$·toluene with: a) RE = Gd, b) RE = Gd, c) RE = Dy, d) RE = Y. Unlabeled atoms are carbon (grey) and hydrogen (white).

Table S2 Selected bond lengths (Å) and angle (°) in **1-Gd**.

O1-C8	1.459(5)	C9-C10	1.481(8)
O1-C11	1.452(6)	C10-C11	1.500(7)
O1-Gd1	2.404(4)	B1-Gd1	2.744(5)
O1-Gd1A	2.334(4)	B1-Gd1[1]	2.744(5)
N1-C7[1]	1.449(6)	B1-Gd1A[1]	2.624(4)
N1-C7	1.449(6)	B1-Gd1A	2.624(4)
N1-B1	1.426(8)	B1-Gd1	2.486(7)
C1-C2	1.464(5)	B1-Gd1A	2.610(7)
C1-C3	1.526(5)	B3-Gd1	2.535(6)
C1-B1	1.546(5)	B3-Gd1A	2.543(5)
C1-Gd1	2.667(5)	C17-C18	1.521(9)
C1-Gd1[1]	2.785(5)	C18-C12	1.3900
C1-Gd1A[1]	2.712(4)	C18-C16	1.3900
C1-Gd1A	2.592(4)	C12-C13	1.3900
C2-C2[1]	1.428(7)	C13-C14	1.3900
C2-C5	1.516(5)	C14-C15	1.3900
C1-Gd1	2.680(5)	C15-C16	1.3900
C1-Gd1[1]	2.727(5)	Gd1-(C$_4$B)$_{cent}$	2.344(27)
C1-Gd1A[1]	2.721(4)	Gd1A-(C$_4$B)$_{cent}$	2.344(27)
C1-Gd1A	2.672(4)	Gd1[1]-(C$_4$B)$_{cent}$	2.4088(42)
C3-C4	1.500(5)	Gd1A[1]-(C$_4$B)$_{cent}$	2.4088(42)
C5-C6	1.519(6)	Gd1-(C$_4$B)$_{cent}$-Gd1A	174.198(91)
C8-C9	1.499(8)	Gd1[1]-(C$_4$B)$_{cent}$-Gd1A[1]	179.400(138)

[1] 1-X,+Y,3/2-Z

Table S3 Selected bond lengths (Å) and angle (°) in **1-Dy**.

Dy1-O1	2.331(2)	C3-C4	1.504(4)
Dy1-C1	2.591(2)	C5-C6	1.523(4)
Dy1-C1[1]	2.703(2)	C8-C9	1.509(5)
Dy1-C2[1]	2.683(2)	C9-C10	1.486(6)
Dy1-C2	2.639(2)	C10-C11	1.501(5)
Dy1-B1	2.6517(19)	C12-C13	1.3900
Dy1-B2	2.534(4)	C12-C17	1.3900
Dy1-B3	2.502(3)	C12-C18	1.500(8)
O1-C8	1.461(3)	C13-C14	1.3900
O1-C11	1.464(4)	C14-C15	1.3900
N1-C7	1.449(4)	C15-C16	1.3900
N1-C7[1]	1.449(4)	C16-C17	1.3900
N1-B1	1.452(5)	Dy1-$(C_4B)_{cent}$	2.3302(4)
C1-C2	1.462(3)	Dy1A-$(C_4B)_{cent}$	2.3302(4)
C1-C3	1.529(3)	Dy1-$(C_4B)_{cent}$-Dy1A	177.448(14)
C1-B1	1.554(3)		
C2-C2[1]	1.434(5)		
C2-C5	1.518(3)		

[1] 1-X,+Y,3/2-Z

Table S4 Selected bond lengths (Å) and angle (°) in **1-Y**.

Y1-O1	2.3164(15)	C2-C5	1.516(3)
Y1-C1[1]	2.5897(17)	C3-C4	1.510(3)
Y1-C1	2.7007(18)	C5-C6	1.516(3)
Y1-C2	2.6765(18)	C8-C9	1.505(4)
Y1-C2[1]	2.6360(17)	C9-C10	1.488(4)
Y1-B1	2.6521(14)	C10-C11	1.511(4)
Y1-B2	2.494(2)	C18-C12	1.502(9)
Y1-B3	2.526(3)	C12-C17	1.3900
O1-C8	1.466(3)	C12-C13	1.3900
O1-C11	1.463(3)	C17-C16	1.3900
N1-C7[1]	1.452(3)	C16-C15	1.3900
N1-C7	1.452(3)	C15-C14	1.3900
N1-B1	1.446(4)	C14-C13	1.3900
C1-C2	1.463(3)	Y1-(C$_4$B)$_{cent}$	2.3270(4)
C1-C3	1.531(3)	Y1A-(C$_4$B)$_{cent}$	2.3270(4)
C1-B1	1.556(3)	Y1-(C$_4$B)$_{cent}$-Y1A	177.705(14)
C2-C2[1]	1.433(4)		

[1] 1-X,+Y,1/2-Z

UV/vis/NIR Spectroscopy

UV/vis/NIR absorption spectra were collected from 200-800 nm on a Shimadzu UV-3600 Plus spectrophotometer at room temperature. The specific procedure was as follows: first, inside an inert atmosphere glovebox, a series of standard solutions of the target compound at different concentrations were prepared using rigorously dehydrated and degassed THF as the solvent. Each solution was then promptly transferred into a quartz cuvette equipped with an air-tight lid and securely sealed. The sealed cuvettes were placed in a sealed container for transfer out of the glovebox and immediately loaded into the sample compartment of the spectrophotometer. The measurement parameters were set in the controlling software with a data interval of 0.5 nm. Using dehydrated and degassed THF in an identical sealed cuvette as the reference, the scans were initiated. Upon completion of the measurements, the cuvettes were promptly returned to the glovebox for cleaning or disposal.

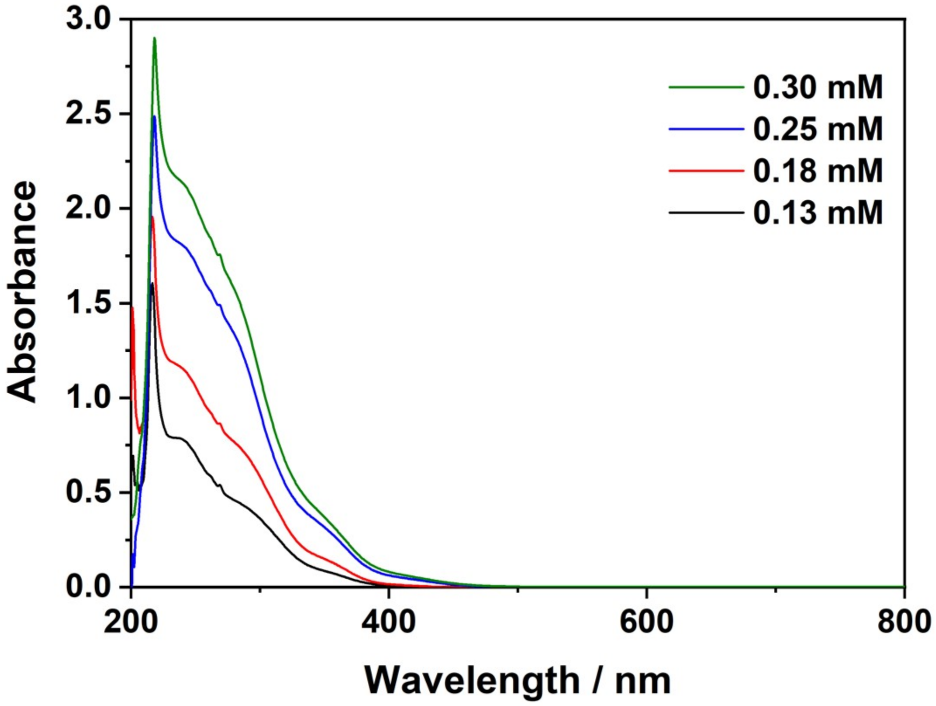

Fig. S5 UV/vis/NIR spectrum of **1-Gd** in tetrahydrofuran at different concentrations. Significant absorptions occur at λ = 218, 242 and 269 nm.

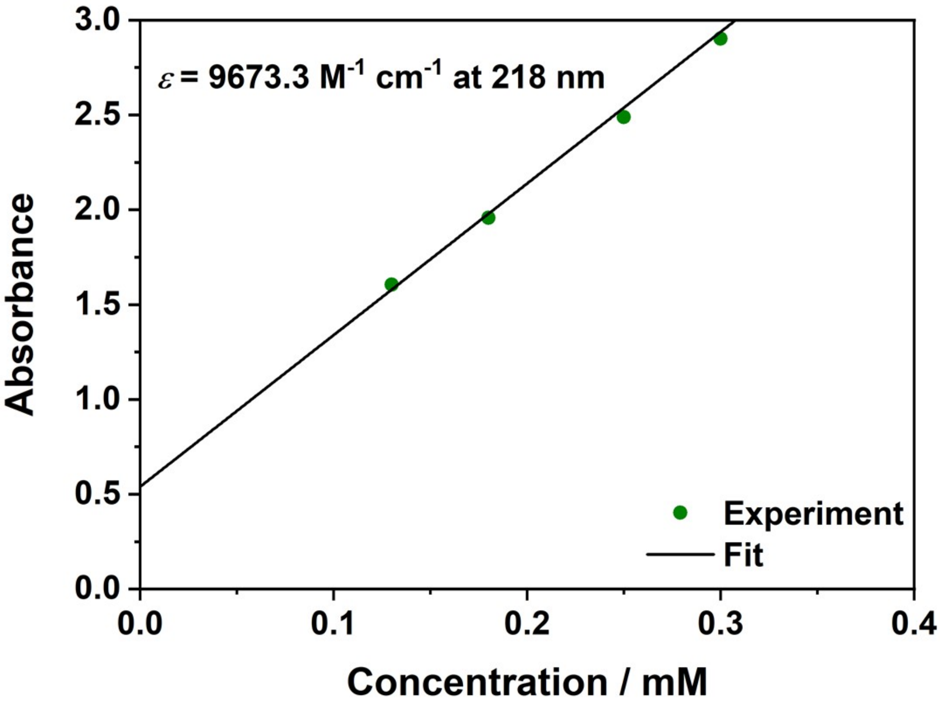

Fig. S6 Plot of absorbance versus concentration for **1-Gd** at 218 nm in the UV/vis/NIR spectrum. The green points are from the UV/vis/NIR spectrum. The solid black line is the best fit to the data to extract the extinction coefficient.

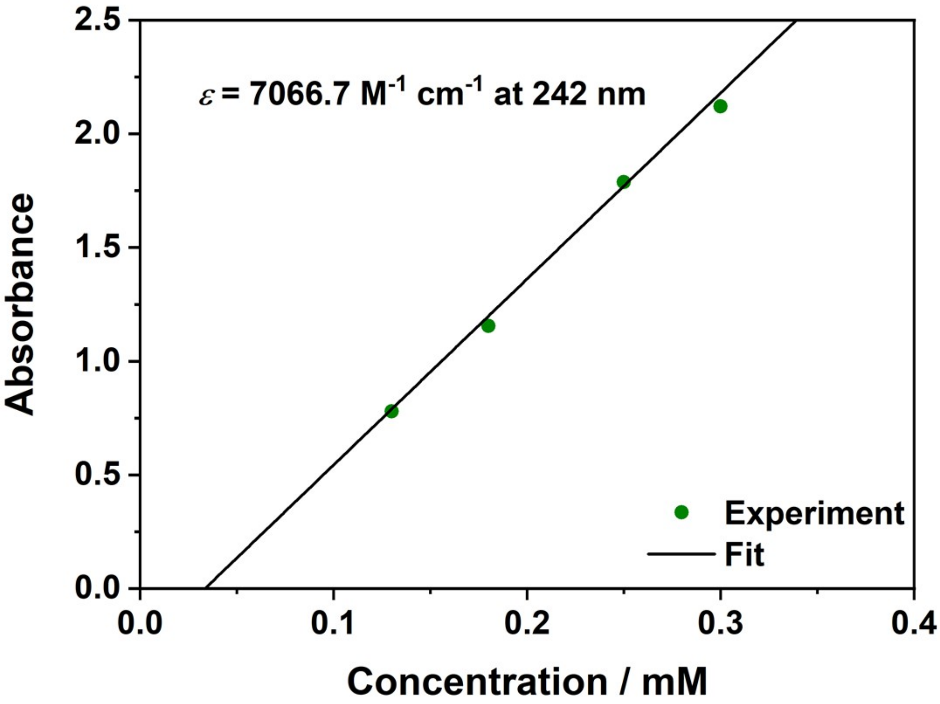

Fig. S7 Plot of absorbance versus concentration for **1-Gd** at 242 nm in the UV/vis/NIR spectrum. The green points are from the UV/vis/NIR spectrum. The solid black line is the best fit to the data to extract the extinction coefficient.

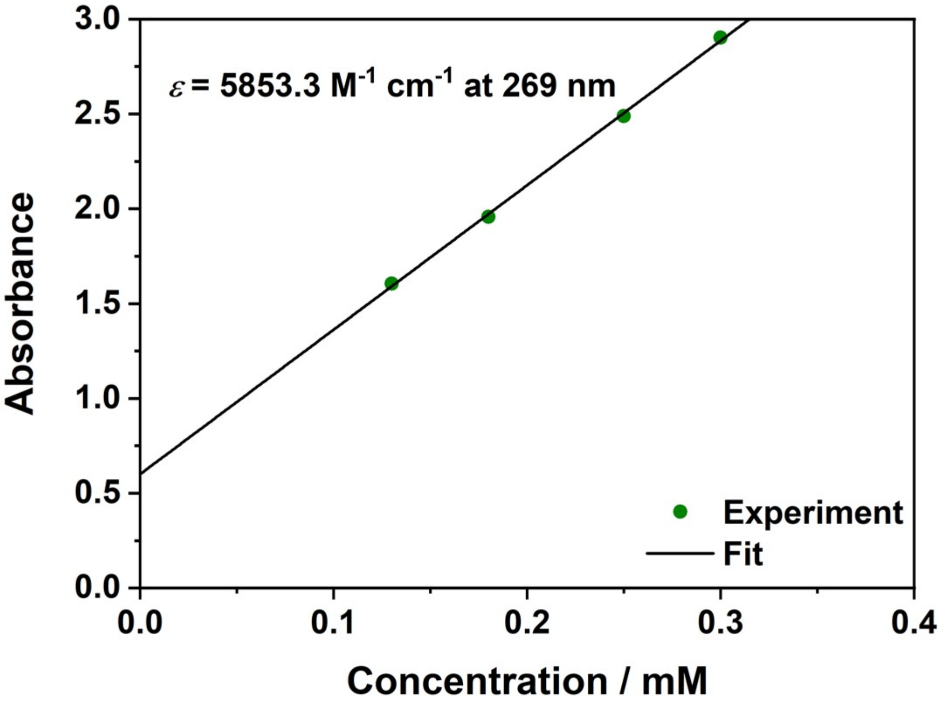

Fig. S8 Plot of absorbance versus concentration for **1-Gd** at 269 nm in the UV/vis/NIR spectrum. The green points are from the UV/vis/NIR spectrum. The solid black line is the best fit to the data to extract the extinction coefficient.

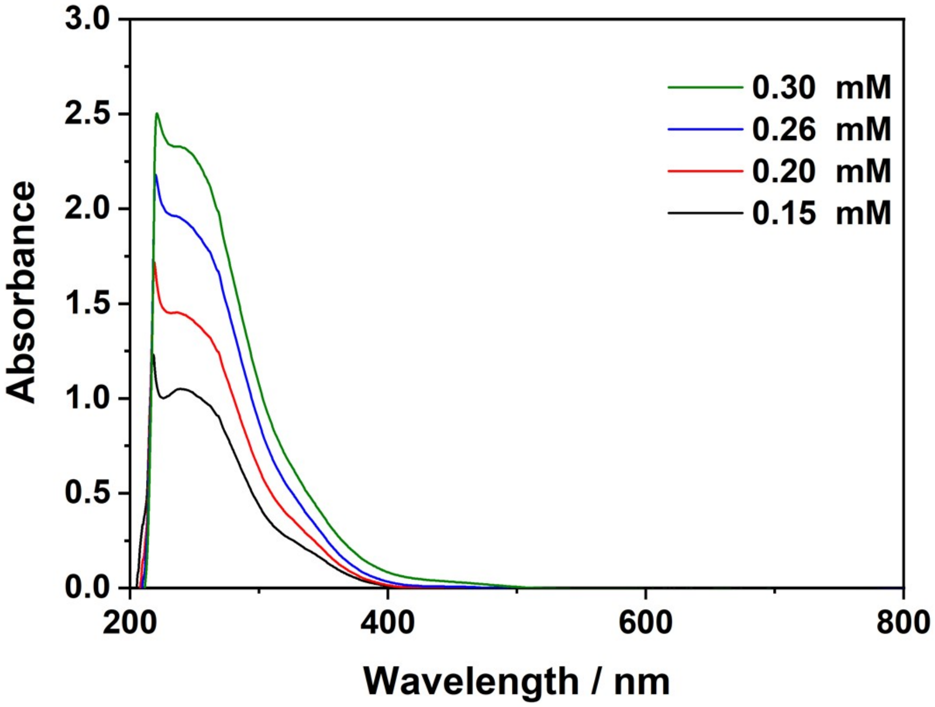

Fig. S9 UV/vis/NIR spectrum of **1-Dy** in tetrahydrofuran at different concentrations. Significant absorptions occur at λ = 221 and 239 nm.

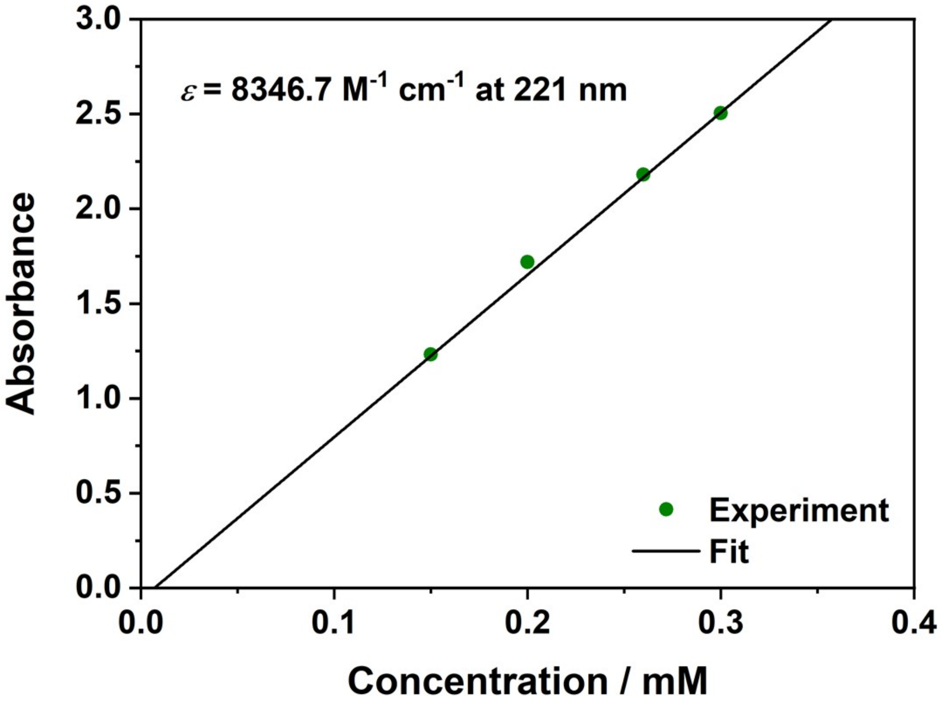

Fig. S10 Plot of absorbance versus concentration for **1-Dy** at 221 nm in the UV/vis/NIR spectrum. The green points are from the UV/vis/NIR spectrum. The solid black line is the best fit to the data to extract the extinction coefficient.

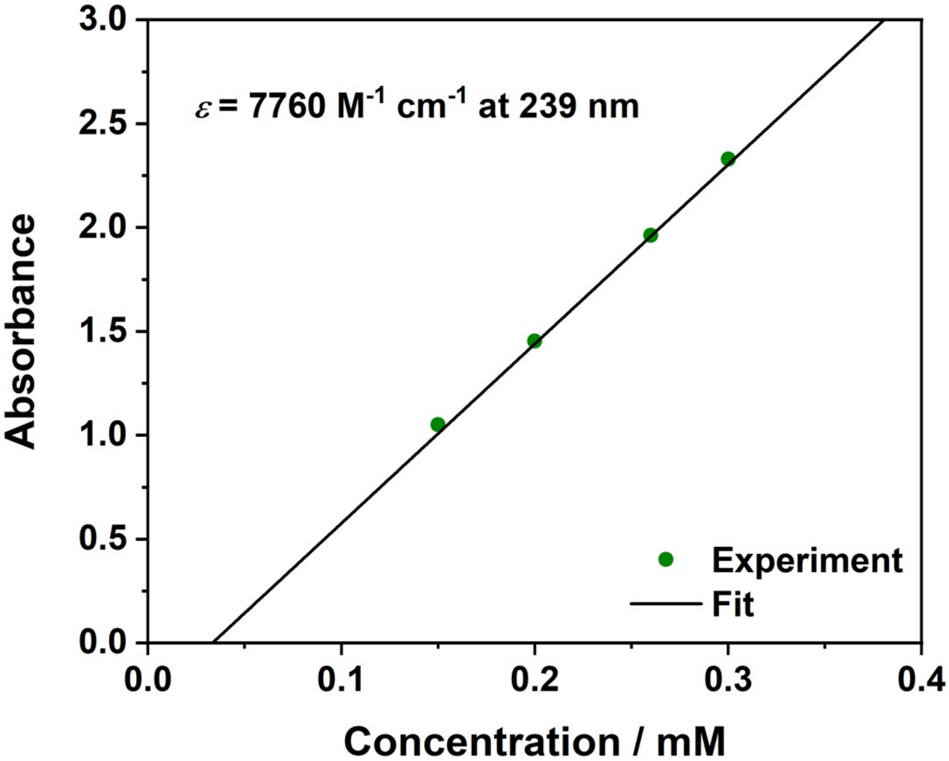

Fig. S11 Plot of absorbance versus concentration for **1-Dy** at 239 nm in the UV/vis/NIR spectrum. The green points are from the UV/vis/NIR spectrum. The solid black line is the best fit to the data to extract the extinction coefficient.

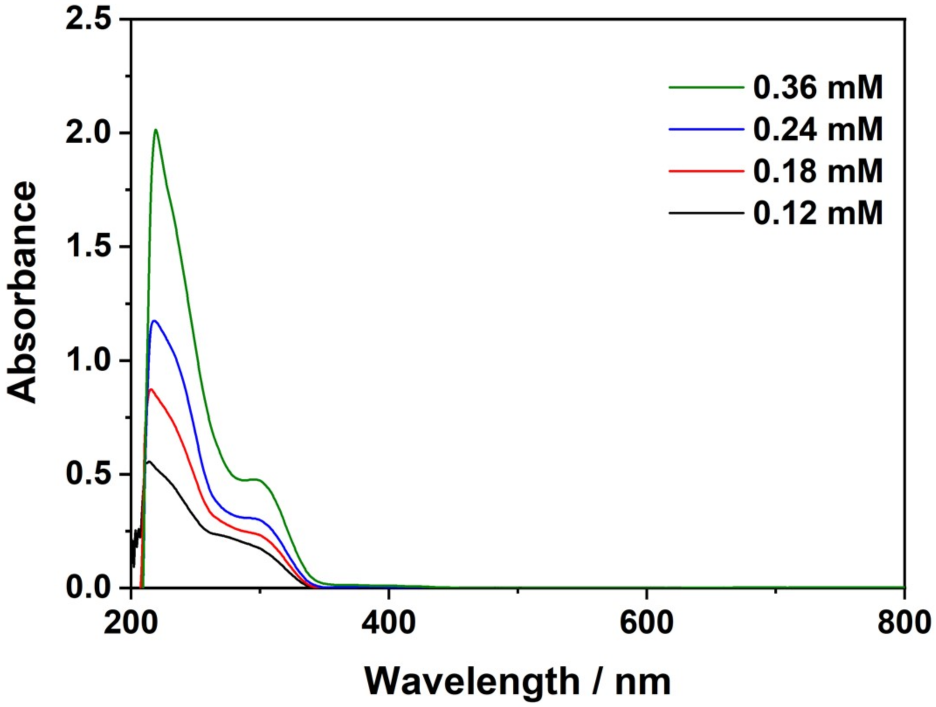

Fig. S12 UV/vis/NIR spectrum of **1-Y** in tetrahydrofuran at different concentrations. Significant absorptions occur at λ = 219 and 299 nm.

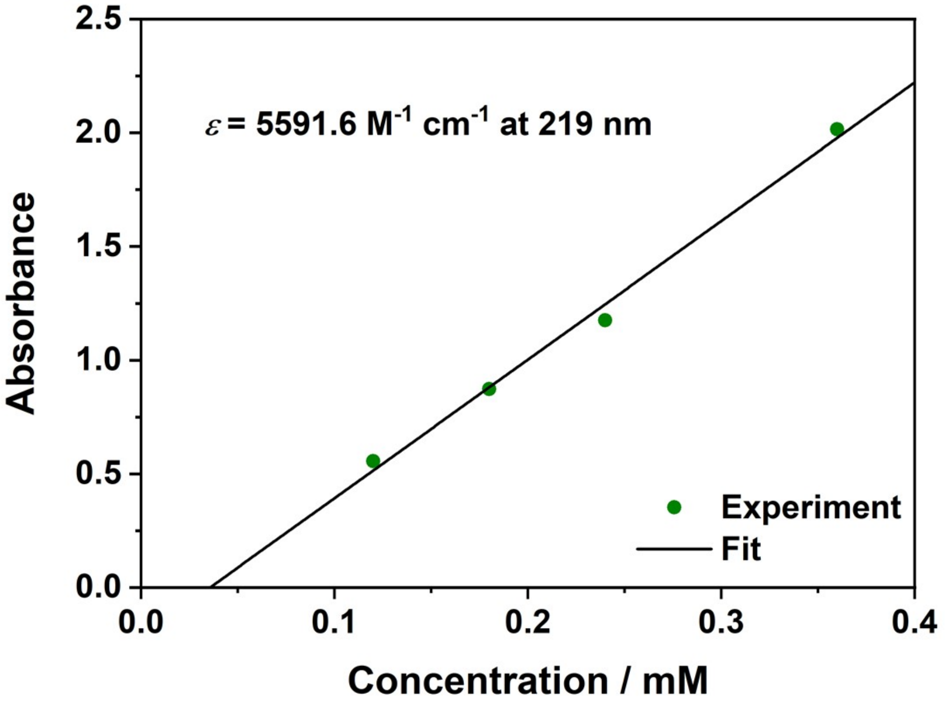

Fig. S13 Plot of absorbance versus concentration for **1-Y** at 219 nm in the UV/vis/NIR spectrum. The green points are from the UV/vis/NIR spectrum. The solid black line is the best fit to the data to extract the extinction coefficient.

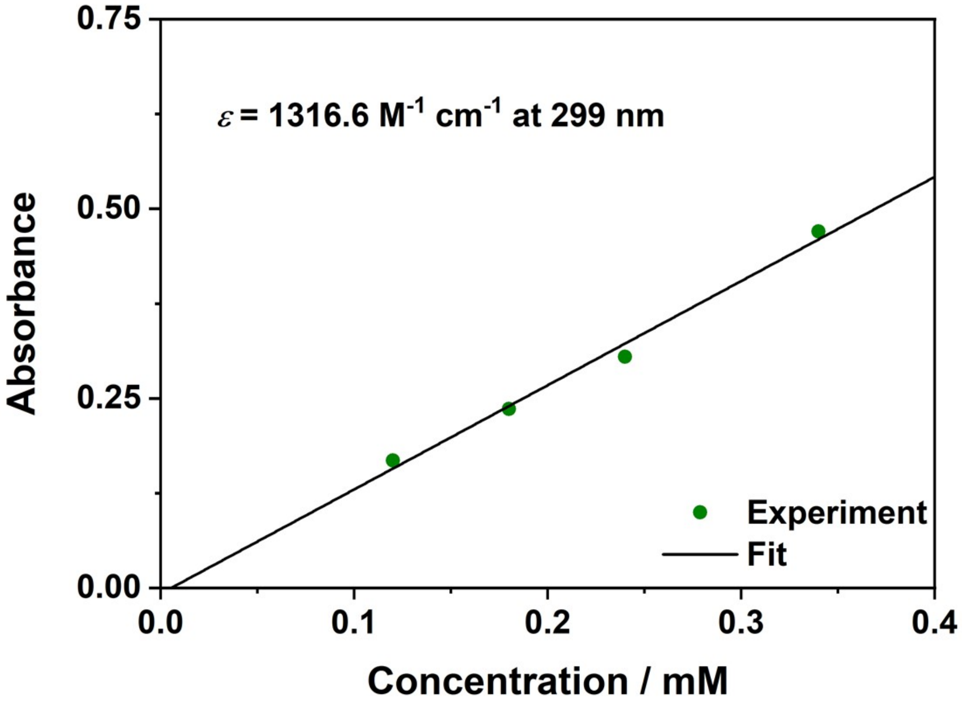

Fig. S14 Plot of absorbance versus concentration for **1-Y** at 299 nm in the UV/vis/NIR spectrum. The green points are from the UV/vis/NIR spectrum. The solid black line is the best fit to the data to extract the extinction coefficient.

The UV-Vis-NIR absorption spectra within the 200−800 nm were collected for the solutions of **1-RE** (THF). The spectra of **1-Gd** displayed intense absorption bands at approximately 218 nm, 242 nm and 269 nm. The spectra of **1-Dy** displayed intense absorption bands at approximately 221 nm and 239 nm. The spectra of **1-Y** displayed intense absorption bands at approximately 219 nm and 299 nm. The spectra of **1-Gd**, **1-Dy**, and **1-Y** (Figures S5−S14) all displayed intense absorption bands at approximately 220 and 270 nm, which can be attributed to the aminoborolide ligand.[4]

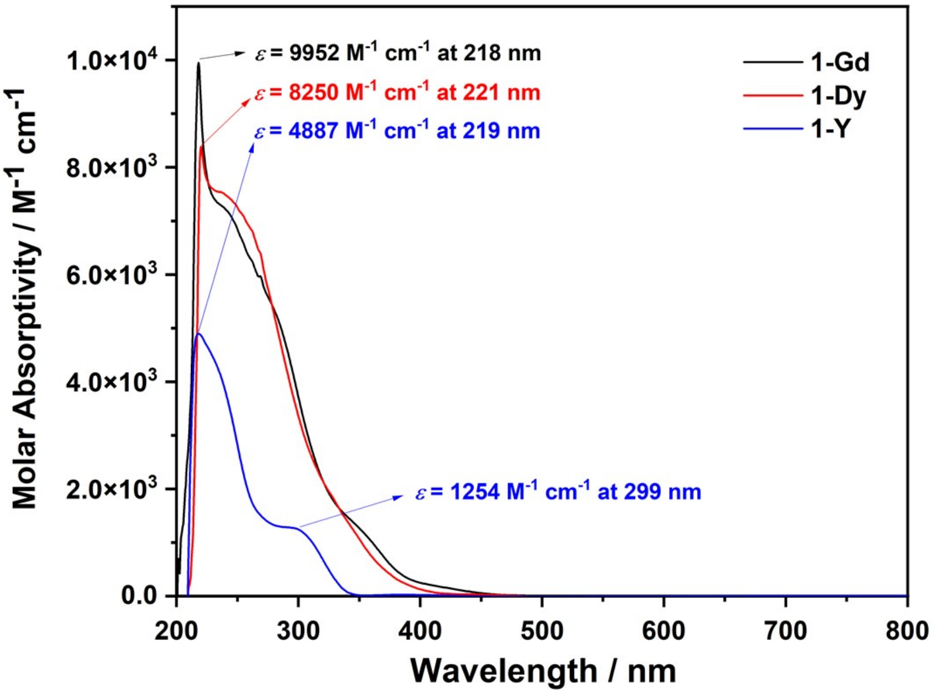

Fig. S15 UV-Vis-NIR spectra of **1-Gd** (THF), **1-Dy** (THF) and **1-Y** (THF) at room temperature.

Magnetic Measurements

The samples of $[(\eta^5\text{-}(C_4B)^{Et4Me2N})RE_2(BH_4)_4(THF)_2]\cdot$toluene (RE = Gd, Dy) were restrained in eicosane and sealed in NMR tubes. The eicosane was melted in a water bath at 40 °C to prevent the orientation of the crystals. Direct current (DC) magnetic susceptibility and magnetization data (VSM mode) were collected using a Quantum Design MPMS3 magnetometer in cooling mode. Alternating current (AC) magnetic susceptibility measurements were performed using a Quantum Design MPMS3 magnetometer using an oscillating field of 2 Oe. Diamagnetic corrections were performed using Pascal's coefficients.[5]

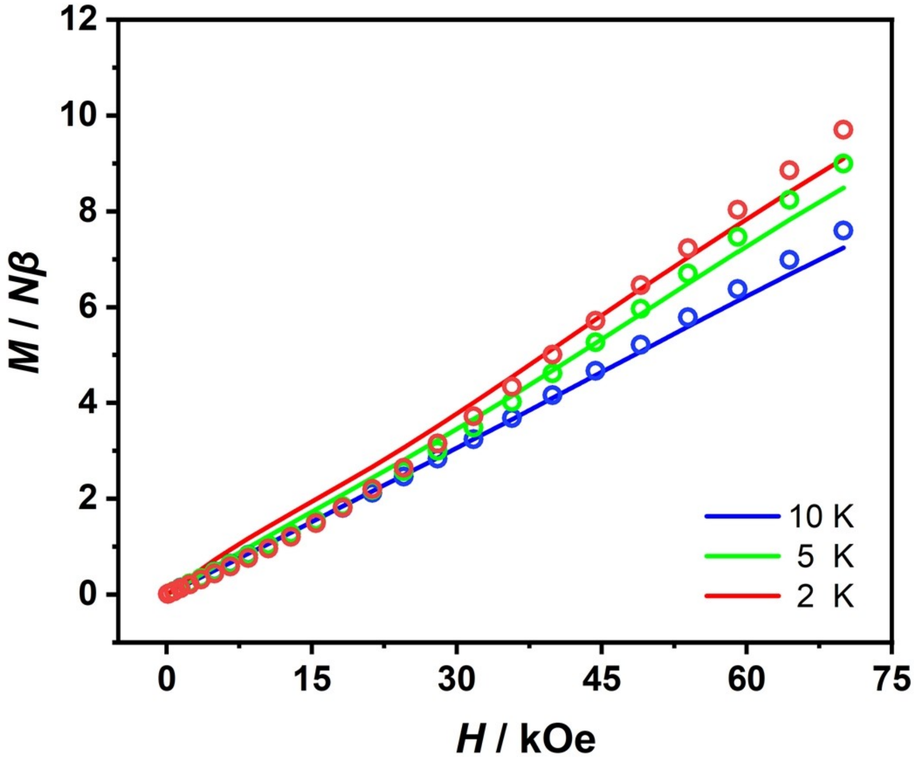

Fig. S16 Field dependence of the magnetization (*M*) at 2 K (red circles), 5 K (green circles), and 10 K (blue circles) for **1-Gd**. Solid lines represent the fitted results. $M = 9.10\ N\beta$ at 2 K and 70 kOe.

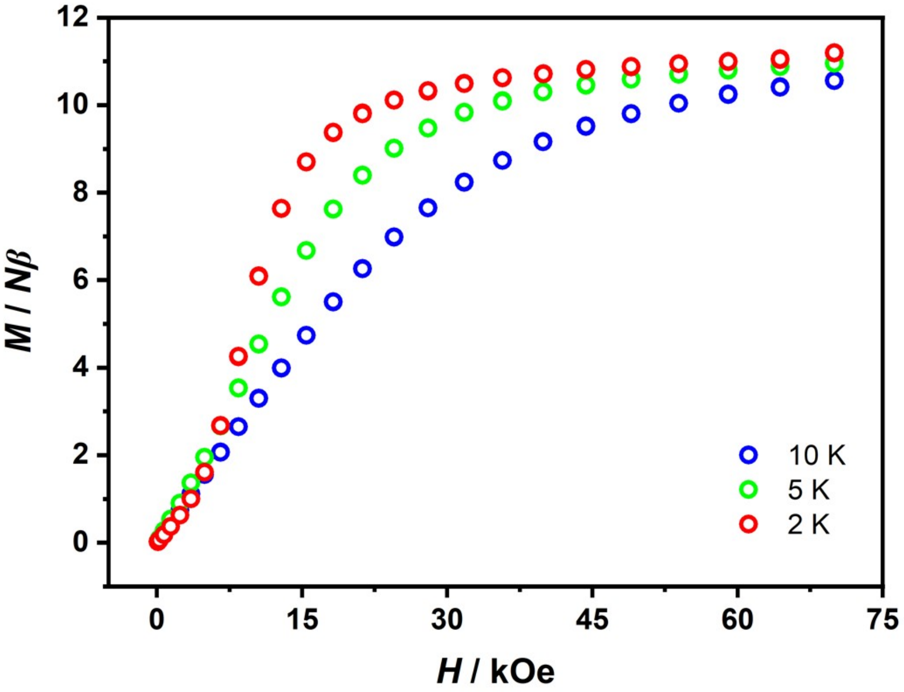

Fig. S17 Field dependence of the magnetization (M) at 2 K (red), 5 K (green), and 10 K (blue) for **1-Dy**. $M = 11.19\ N\beta$ at 2 K and 70 kOe.

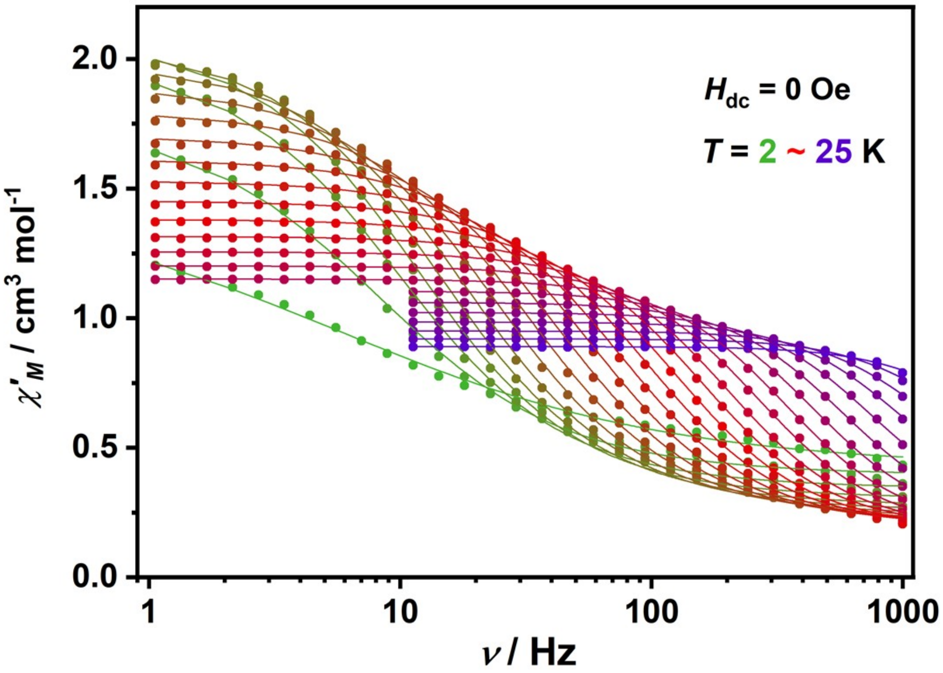

Fig. S18 Frequency dependence of the in-phase susceptibility (χ'_{M}) for **1-Dy** in zero DC field at AC frequencies of 1-999 Hz from 2 to 25 K. Solid lines are a guide to the eye. Solid lines represent fits of the data using the generalized Debye model, which describe χ' and χ'' in terms of frequency, isothermal susceptibility (χ_∞), adiabatic susceptibility (χ_{S}), relaxation time (τ), and a variable representing the distribution of relaxation times (α).

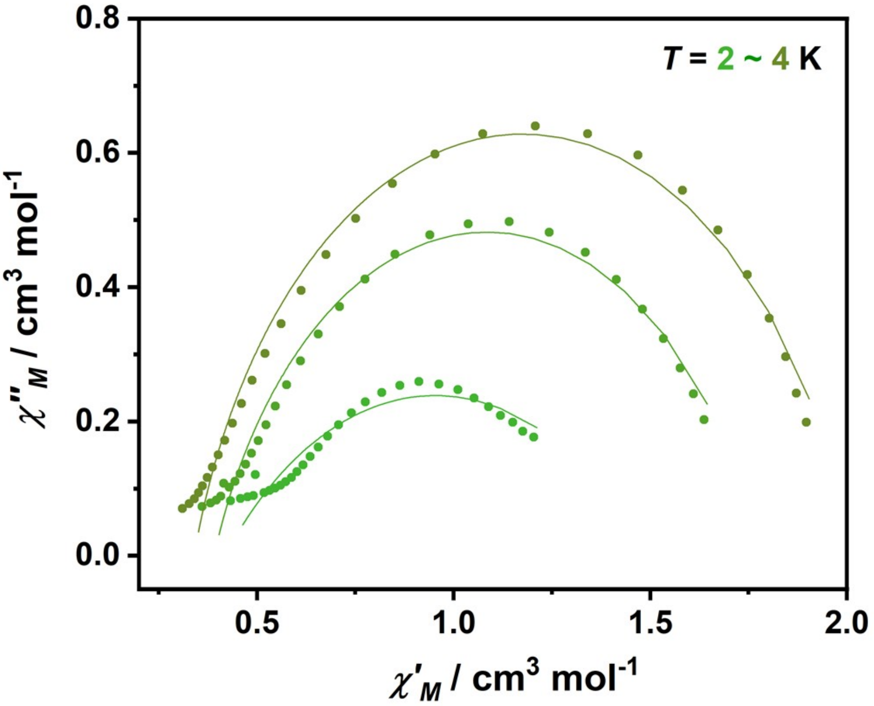

Fig. S19 Cole−Cole plots for the AC susceptibilities in zero DC field for **1-Dy** from 2-4 K. Solid lines represent fits of the data in Fig. S18 and Fig. 3a using the generalized Debye model.

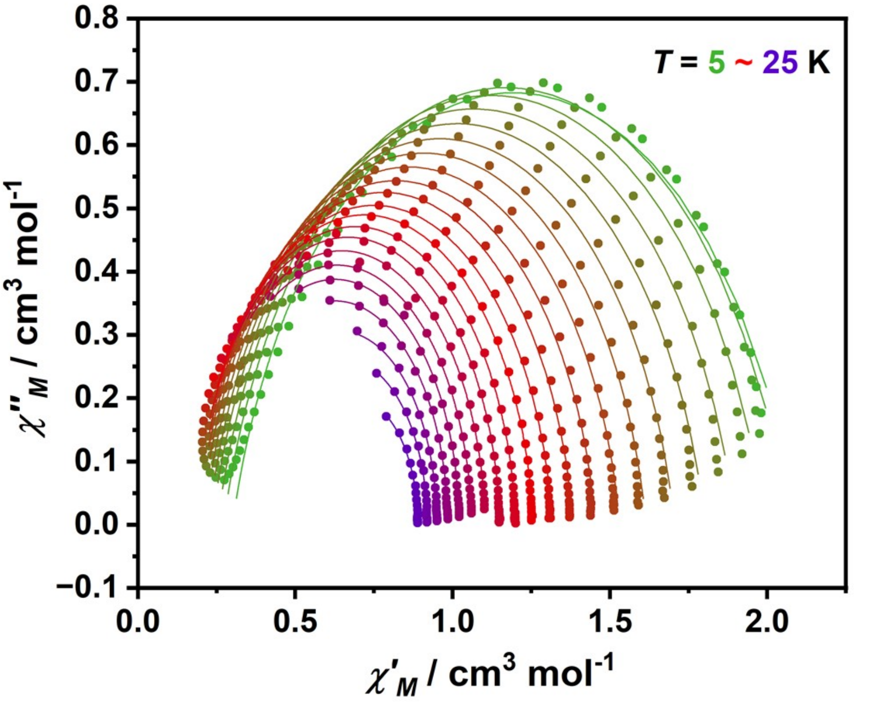

Fig. S20 Cole−Cole plots for the AC susceptibilities in zero DC field for **1-Dy** from 5-25 K. Solid lines represent fits of the data in Fig. S18 and Fig. 3a using the generalized Debye model.

Table S5 Relaxation fitting parameters for **1-Dy** corresponding to Fig. S19-20 using the generalized Debye model.

T / K	χ_T / cm^3 mol^{-1}	χ_S / cm^3 mol^{-1}	α	τ / s
2	1.48812(0.03407)	0.41875(0.01089)	0.46543(0.01938)	0.02854(0.00278)
3	1.77782(0.0149)	0.39131(0.00668)	0.22648(0.01042)	0.01947(4.74235E-4)
4	2.01105(0.01246)	0.34035(0.00641)	0.17913(0.00802)	0.01641(2.72374E-4)
5	2.08666(0.01224)	0.30076(0.00702)	0.16883(0.00785)	0.01376(2.16084E-4)
6	2.06446(0.01183)	0.27232(0.00765)	0.16391(0.00807)	0.01118(1.7662E-4)
7	1.99136(0.01076)	0.25281(0.00826)	0.15619(0.00821)	0.00876(1.37007E-4)
8	1.89995(0.0091)	0.2359(0.00777)	0.14889(0.00777)	0.00667(9.77057E-5)
9	1.80188(0.00763)	0.22378(0.00755)	0.13847(0.00744)	0.005(6.89204E-5)
10	1.70489(0.00611)	0.21192(0.00699)	0.12782(0.0068)	0.00374(4.63718E-5)
11	1.61456(0.00481)	0.20037(0.00633)	0.11768(0.00608)	0.00281(3.07717E-5)
12	1.53079(0.0037)	0.19221(0.00558)	0.10712(0.00529)	0.00214(2.0187E-5)
13	1.45321(0.00304)	0.18712(0.00525)	0.09673(0.00492)	0.00164(1.42956E-5)
14	1.38185(0.00228)	0.1814(0.00449)	0.08507(0.00415)	0.00127(9.27514E-6)
15	1.31633(0.00216)	0.18514(0.00487)	0.07252(0.00446)	0.001(7.79634E-6)
16	1.25605(0.0019)	0.18378(0.00494)	0.0579(0.00444)	7.87732E-4(6.06833E-6)
17	1.2016(0.00125)	0.17897(0.0039)	0.05238(0.00334)	6.01344E-4(3.59264E-6)
18	1.15059(6.85418E-4)	0.18496(0.00256)	0.039(0.00211)	4.67925E-4(1.81444E-6)
19	1.10435(0.00228)	0.19314(0.0074)	0.0327(0.00615)	3.59551E-4(3.97253E-6)
20	1.06115(0.00168)	0.20542(0.00727)	0.02712(0.00557)	2.75268E-4(3.09914E-6)
21	1.02116(9.6941E-4)	0.23067(0.00573)	0.01254(0.00407)	2.12386E-4(1.97923E-6)
22	0.98459(9.28914E-4)	0.2705(0.00788)	0.00648(0.00516)	1.63531E-4(2.30392E-6)
23	0.94964(7.89244E-4)	0.33849(0.00946)	0(0.00609)	1.30571E-4(2.56365E-6)
24	0.91928(7.83873E-4)	0.39796(0.0141)	0(0.00867)	1.02316E-4(3.51844E-6)
25	0.88945(7.9234E-4)	0.49251(0.01898)	0(0.01328)	8.68773E-5(5.27303E-6)

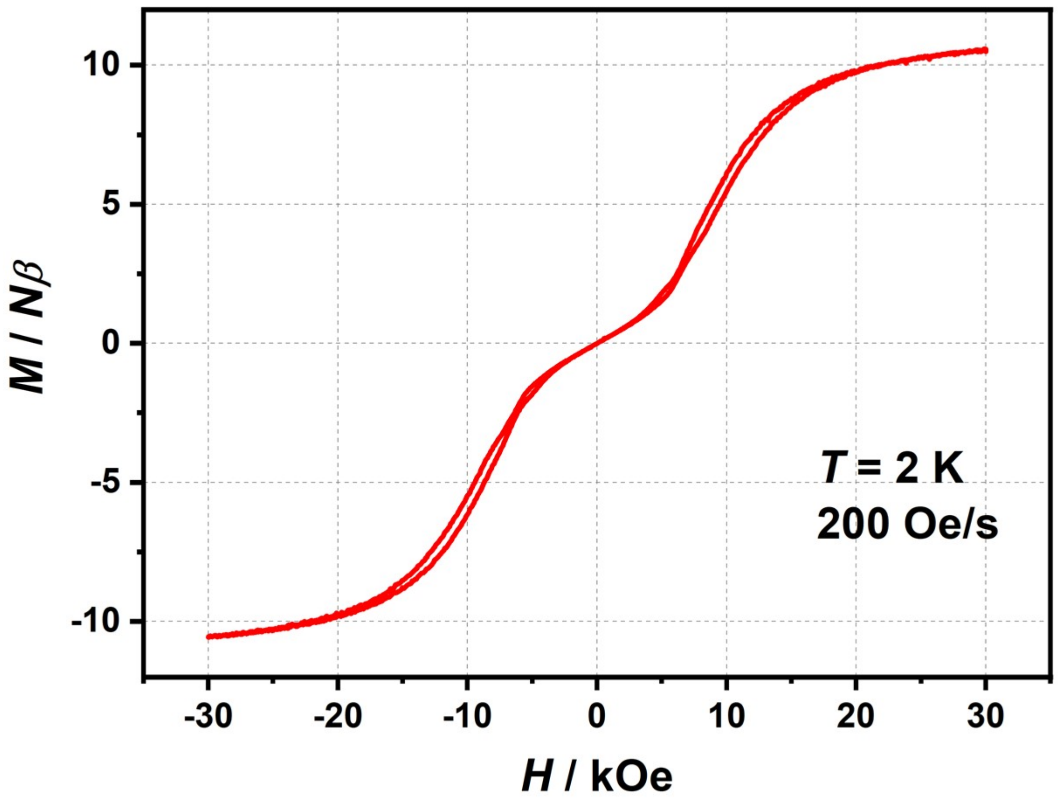

Fig. S21 Magnetic hysteresis loops for **1-Dy**. The data were collected continuously at 2 K using a field sweep speed of 200 Oe s^{-1}.

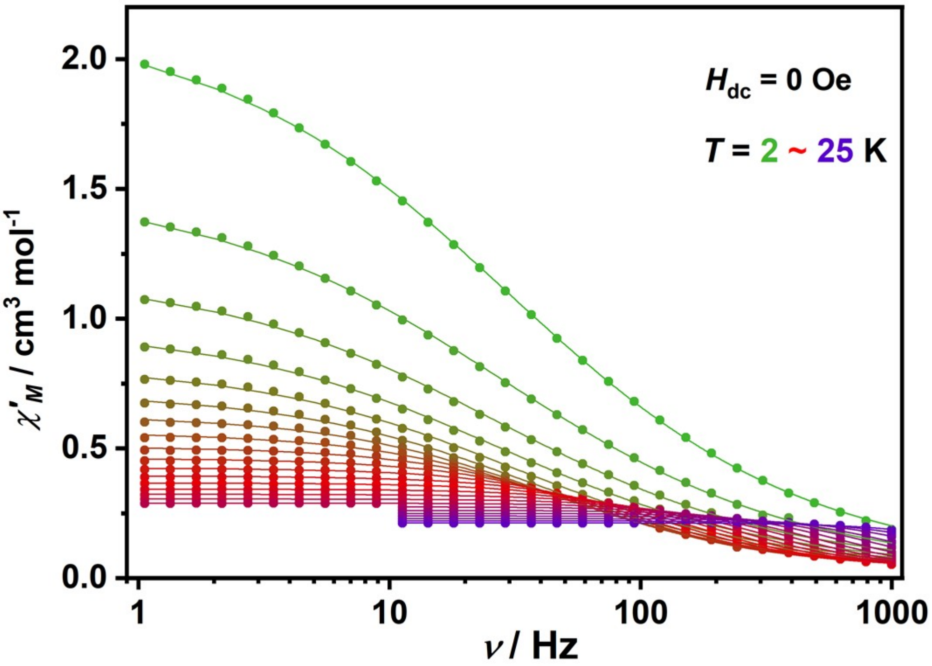

Fig. S22 Frequency dependence of the in-phase susceptibility (χ'_M) for **1-Dy@Y** in zero DC field at AC frequencies of 1-999 Hz from 2 to 25 K. Solid lines are a guide to the eye. Solid lines represent fits of the data using the generalized Debye model, which describe χ' and χ'' in terms of frequency, isothermal susceptibility (χ_∞), adiabatic susceptibility (χ_S), relaxation time (τ), and a variable representing the distribution of relaxation times (α).

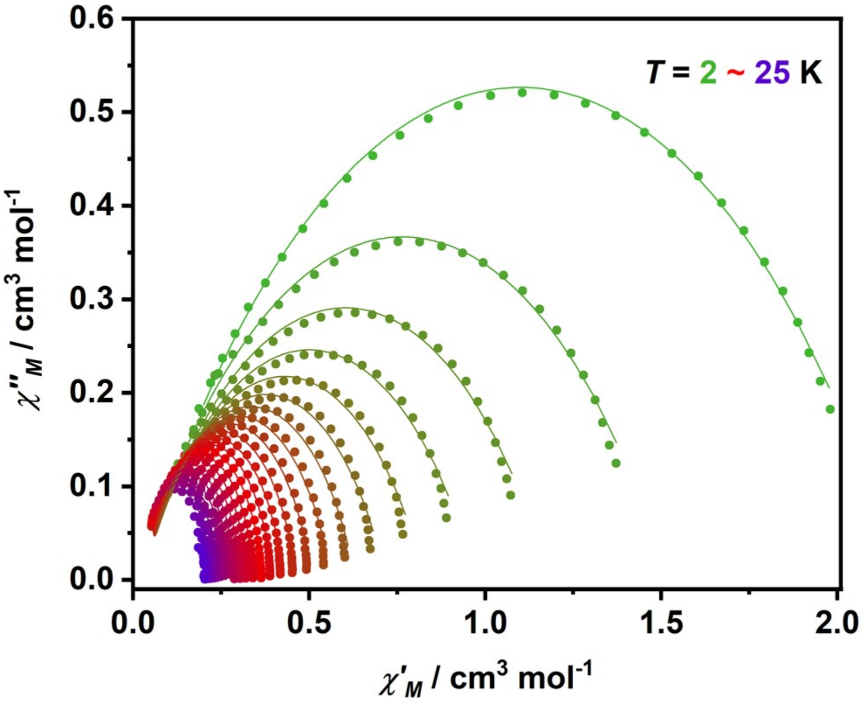

Fig. S23 Cole−Cole plots for the AC susceptibilities in zero DC field for **1-Dy@Y** from 2-25 K. Solid lines represent fits of the data in Fig. S22 and Fig. 3c using the generalized Debye model.

Table S6 Relaxation fitting parameters for **1-Dy@Y** corresponding to Fig. S23 using the generalized Debye model.

T / K	χ_T / cm^3 mol^{-1}	χ_S / cm^3 mol^{-1}	α	τ / s
2	2.17369(0.00522)	0.02497(0.00492)	0.41986(0.00275)	0.00538(4.50882E-5)
3	1.51445(0.00626)	0.01608(0.00571)	0.42048(0.00465)	0.00567(8.06234E-5)
4	1.181(0.00574)	0.02338(0.00511)	0.4072(0.00557)	0.00589(9.76454E-5)
5	0.97355(0.00557)	0.02649(0.00506)	0.39025(0.00684)	0.00572(1.12509E-4)
6	0.82807(0.00525)	0.03032(0.00502)	0.36456(0.00813)	0.00527(1.16818E-4)
7	0.71797(0.00464)	0.03365(0.00482)	0.33186(0.00911)	0.0046(1.072E-4)
8	0.63182(0.00389)	0.03704(0.00448)	0.291(0.00969)	0.00384(8.88189E-5)
9	0.56307(0.00307)	0.03902(0.00397)	0.25096(0.00955)	0.00311(6.65529E-5)
10	0.50763(0.00235)	0.03884(0.00342)	0.21258(0.00893)	0.00248(4.68047E-5)
11	0.46274(0.00182)	0.03874(0.00298)	0.18166(0.00826)	0.00196(3.2939E-5)
12	0.4254(0.00135)	0.03721(0.00248)	0.15506(0.00716)	0.00156(2.19077E-5)
13	0.39404(0.00102)	0.03604(0.00213)	0.1338(0.00631)	0.00124(1.5026E-5)
14	0.36693(7.63355E-4)	0.03521(0.00178)	0.11107(0.00542)	9.95908E-4(1.0134E-5)
15	0.34331(5.58365E-4)	0.0345(0.00148)	0.09278(0.00455)	7.96831E-4(6.74146E-6)
16	0.32299(4.25842E-4)	0.03378(0.0013)	0.07783(0.00396)	6.40089E-4(4.7413E-6)
17	0.30492(4.28887E-4)	0.03464(0.00152)	0.06355(0.00459)	5.18252E-4(4.50189E-6)
18	0.28875(2.44907E-4)	0.03366(0.00103)	0.04681(0.00302)	4.12416E-4(2.41847E-6)
19	0.27426(4.21509E-4)	0.03557(0.0015)	0.03316(0.00455)	3.29462E-4(2.80219E-6)
20	0.26071(3.45308E-4)	0.03999(0.00157)	0.01516(0.00455)	2.6299E-4(2.41549E-6)
21	0.24906(3.12127E-4)	0.04319(0.0019)	0.00922(0.0051)	2.07816E-4(2.44449E-6)
22	0.23904(6.17012E-4)	0.04416(0.0053)	0.01088(0.01265)	1.6219E-4(5.68322E-6)
23	0.22904(4.15543E-4)	0.05754(0.00505)	0(0.0115)	1.29436E-4(4.8367E-6)
24	0.21999(4.22626E-4)	0.07677(0.00707)	0(0.01642)	1.06716E-4(6.70102E-6)
25	0.21198(2.51504E-4)	0.08166(0.00743)	0(0.01426)	7.73412E-5(5.57955E-6)

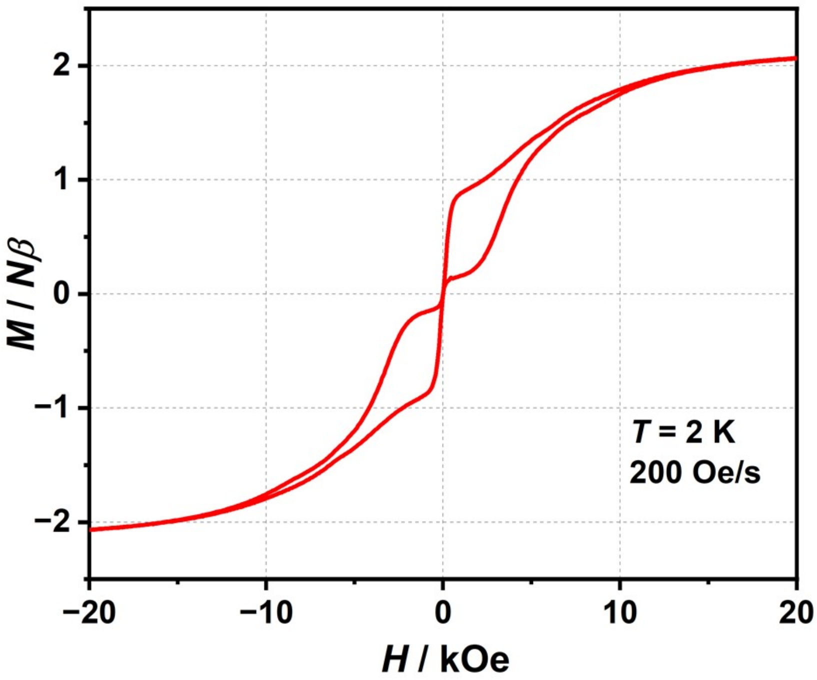

Fig. S24 Magnetic hysteresis loops for **1-Dy@Y**. The data were collected continuously at 2 K using a field sweep speed of 200 Oe s^{-1}.

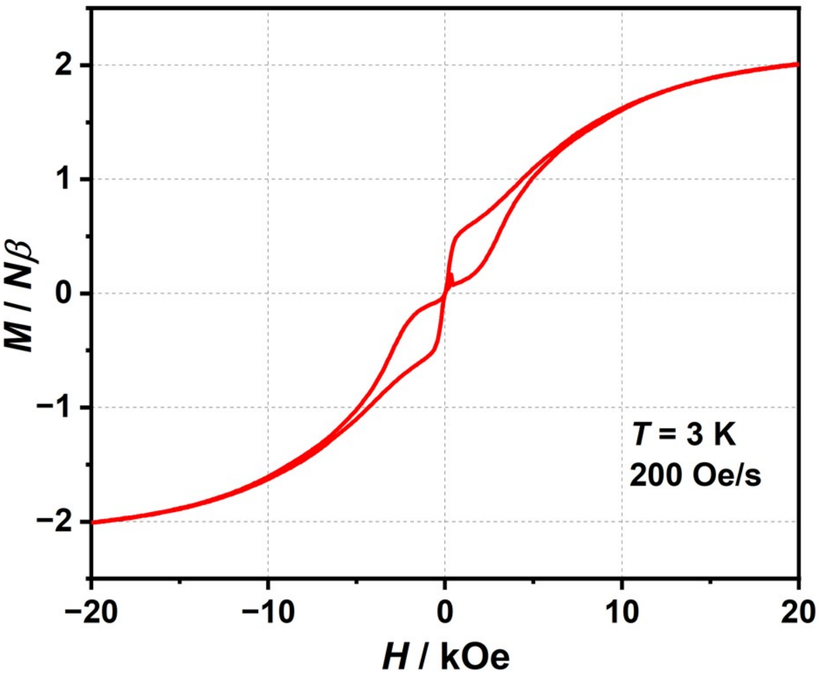

Fig. S25 Magnetic hysteresis loops for **1-Dy@Y**. The data were collected continuously at 3 K using a field sweep speed of 200 Oe s^{-1}.

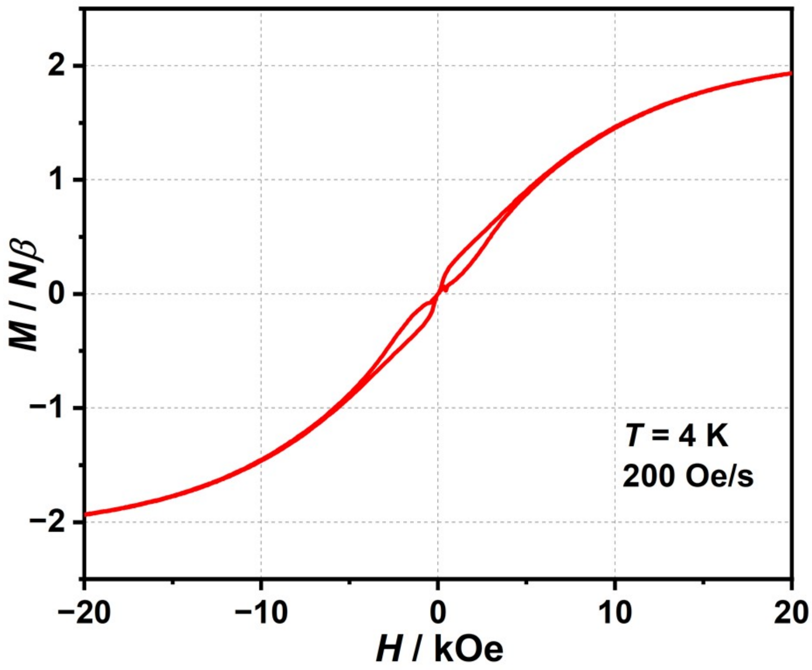

Fig. S26 Magnetic hysteresis loops for **1-Dy@Y**. The data were collected continuously at 4 K using a field sweep speed of 200 Oe s^{-1}.

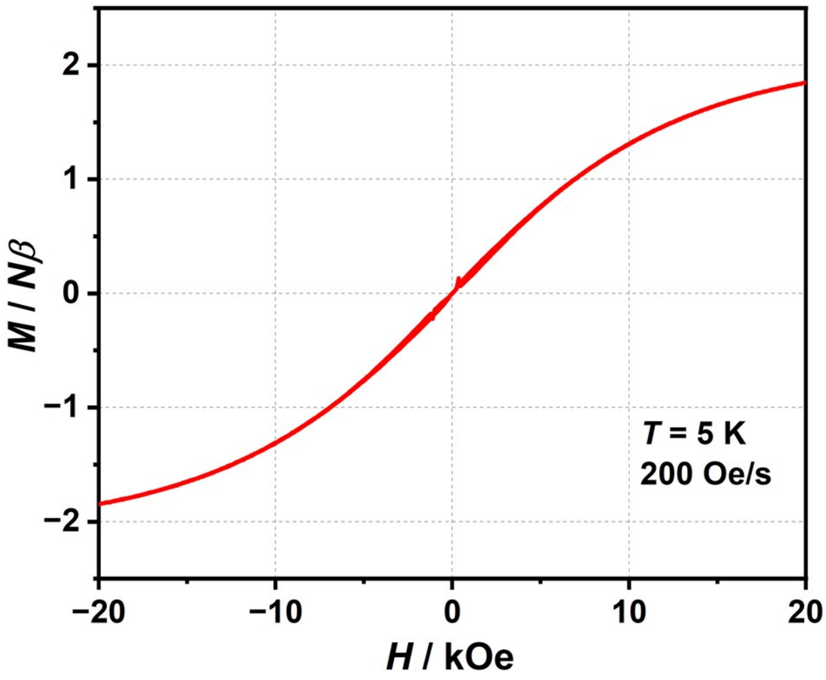

Fig. S27 Magnetic hysteresis loops for **1-Dy@Y**. The data were collected continuously at 5 K using a field sweep speed of 200 Oe s^{-1}.

Computational details

For binuclear complex **1-Dy**, we only need to calculate one individual Dy(III) fragment (**1-Dy'**) due to the central symmetrical structure. Complete-active-space self-consistent field (CASSCF) calculations on **1-Dy'** (see Fig. S28) on the basis of single-crystal X-ray determined geometries have been carried out with OpenMolcas[6] program package. The calculations were performed with the other Dy(III) ion replaced by the diamagnetic Lu(III) keeping the experimentally determined structure. The basis sets for all atoms are atomic natural orbitals from the ANO-RCC library: ANO-RCC-VTZP for Dy; VTZ for close C，B and O; VDZ for distant atoms. The calculations employed the second order Douglas-Kroll-Hess Hamiltonian, where scalar relativistic contractions were taken into account in the basis set and the spin-orbit couplings were handled separately in the restricted active space state interaction (RASSI-SO) procedure.[7,8] Active electrons in 7 active orbitals include all f electrons (CAS (9, 7) for Dy) in the CASSCF calculation. To exclude all the doubts, we calculated all the roots in the active space. We have mixed the maximum number of spin-free state which was possible with our hardware (all from 21 sextets, 128 from 224 quadruplets, 130 from 490 doublets) for each complex. SINGLE_ANISO[9-11] program was used to obtain the energy levels, ***g*** tensors, magnetic axes, *et al.* based on the above CASSCF/RASSI-SO calculations.

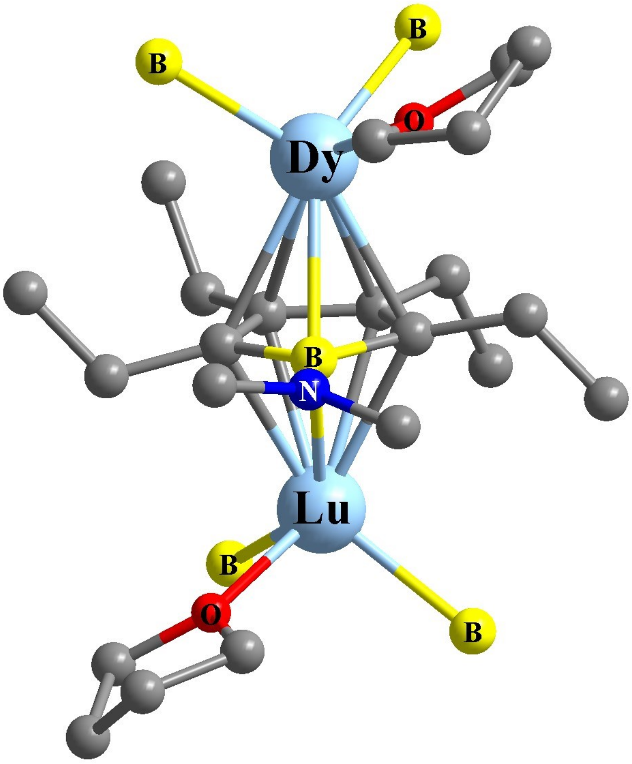

1-Dy'

Fig. S28 Calculated model structure of individual Dy(III) fragment for complex **1-Dy**; H atoms are omitted for clarify.

Table S7 Calculated energy levels (cm^{-1}), ***g*** (g_x, g_y, g_z) tensors and predominant m_J values of the lowest eight Kramers doublets (KDs) of **1-Dy’** using CASSCF/RASSI-SO with OpenMolcas.

KDs	**1-Dy’**		
	E	***g***	m_J
1	0.0	0.005 0.008 19.768	±15/2
2	185.6	0.077 0.176 17.424	±13/2
3	249.1	0.762 1.253 13.286	±11/2
4	286.6	0.111 1.851 13.240	±9/2
5	331.6	2.974 4.167 10.552	±7/2
6	400.7	1.394 5.068 10.010	±5/2
7	479.1	2.998 4.666 6.636	±3/2
8	516.6	11.512 9.113 1.271	±1/2

Table S8 Wave functions with definite projection of the total moment $|m_J>$ for the lowest eight KDs of **1-Dy’** using CASSCF/RASSI-SO with OpenMolcas.

<table>
<tr><th></th><th><i>E</i>/cm^{−1}</th><th>wave functions</th></tr>
<tr><td rowspan="8">1-Dy’</td><td>0.0</td><td>98.5%|±15/2></td></tr>
<tr><td>185.6</td><td>74.7%|±13/2>+17.0%|±11/2>+4.1%|±7/2></td></tr>
<tr><td>249.1</td><td>42.1%|±11/2>+33.0%|±9/2>+17.0%|±13/2>+3.0%|±5/2></td></tr>
<tr><td>286.6</td><td>45.2%|±9/2>+21.1%|±11/2>+14.6%|±7/2>+7.9%|±5/2>+4.4%|±3/2></td></tr>
<tr><td>331.6</td><td>68.0%|±7/2>+12.6%|±11/2>+8.1%|±9/2>+4.3%|±13/2>+3.9%|±5/2></td></tr>
<tr><td>400.7</td><td>71.3%|±5/2>+10.1%|±3/2>+6.8%|±9/2>+5.8%|±7/2>+5.0%|±11/2></td></tr>
<tr><td>479.1</td><td>72.9%|±3/2>+10.0%|±5/2>+8.7%|±1/2>+4.2%|±7/2>+3.2%|±9/2></td></tr>
<tr><td>516.6</td><td>84.0%|±1/2>+8.5%|±3/2>+3.5%|±5/2>+2.0%|±7/2></td></tr>
</table>

Table S9 Calculated crystal-field parameters B(*k*, *q*) for **1-Dy'**.

k	*q*	Weight	*k*	*q*	Weight
2	–2	2.57%	6		
	–1	3.20%		–6	0.33%
	0	26.61%		–5	4.58%
	1	0.13%		–4	2.53%
	2	3.46%		–3	3.62%
4	–4	3.42%		–2	2.18%
	–3	1.59%		–1	4.72%
	–2	2.43%		0	6.56%
	–1	2.08%		1	1.22%
	0	0.87%		2	3.47%
	1	0.75%		3	1.60%
	2	1.60%		4	0.51%
	3	6.42%		5	5.01%
	4	2.69%		6	3.90%

According to the method for the prediction of tunneling demagnetization time (τ_{QTM}) proposed by Yin,[12] we calculated the value of τ_{QTM} according to equations below:

$$\tau_{QTM} = \frac{1}{2k} \tag{S1}$$

$$k = \frac{\beta B_{ave}}{h} \frac{g_{XY}^2}{2(g_{XY}^2 + g_Z^2)^{1/2}} \tag{S2}$$

Where $g_{XY}^2 = (g_X^2 + g_Y^2)$, *k* is the rate of ground state QTM. As usual, the magnitude of the magnetic fields, arising from both dipolar and hyperfine interactions, is of a few tens of mini-Tesla (mT). Thus, in this work, B_{ave} is set to be 20 mT.

Table S10 Values of B_{ave}, principal values of the ***g***-tensor of the lowest KD and the τ_{QTM} for **1-Dy'**.

B_{ave} (mT)	g_{X}	g_{Y}	g_{Z}	τ_{QTM} (s)
20	0.5167×10^{-2}	0.7989×10^{-2}	19.7680	7.80×10^{-3}

To fit the exchange interactions between magnetic centres in complex **1-Dy**, we took two steps to obtain them. Firstly, we calculated individual Dy(III) fragment using CASSCF/RASSI-SO to obtain the corresponding magnetic properties. Then, the exchange interaction between the magnetic centres was considered within the Lines model,[13] while the account of the dipole-dipole magnetic coupling is treated exactly. The Lines model is effective and has been successfully used widely in the research field of d and f-elements single-molecule magnets.[14,15]

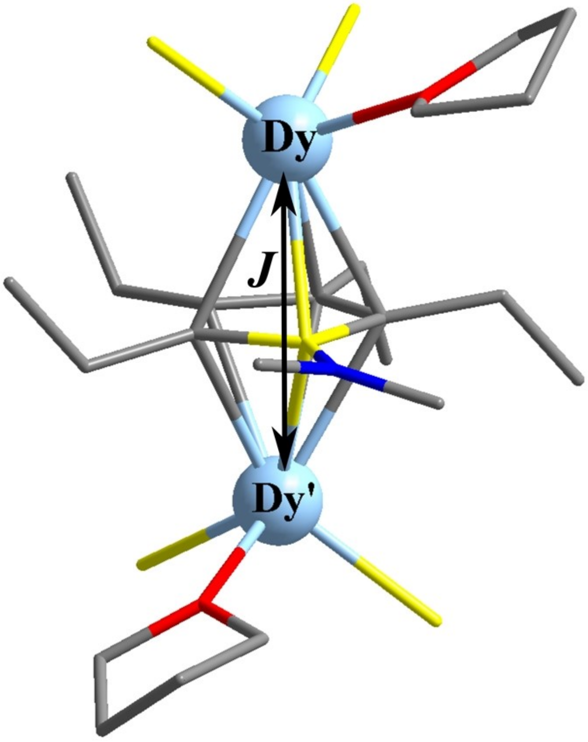

Fig. S29 Scheme of the Dy···Dy interactions in complex **1-Dy**.

The Ising exchange Hamiltonian for **1-Dy** is:

$$\hat{H}_{exch} = -\tilde{J}_{exch}\hat{\tilde{S}}_{Dy}\hat{\tilde{S}}_{Dy'}$$

The $\tilde{J}_{exch} = 25\cos\varphi J_{exch}$, where φ is the angle between the anisotropy axes on two Dy sites, and J_{exch} is the Lines exchange coupling parameter. $\tilde{S}_{Dy}$= 1/2 is the ground pseudospin of the Dy(III). $\tilde{J}_{total}$ is the parameter of the total magnetic interaction ($\tilde{J}_{total} = \tilde{J}_{dip} + \tilde{J}_{exch}$) between magnetic center ions. The dipolar magnetic coupling can be calculated exactly, while the Lines exchange coupling constants were fitted through comparison of the computed and measured magnetic susceptibilities using the POLY_ANISO program,[9-11] and the magnetic susceptibility could be well fitted when the intermolecular interaction zJ' = -0.02 cm^{-1}.

Table S11 Exchange energies *E* (cm^{-1}), the energy difference between each exchange doublets Δ_t (cm^{-1}) and the main values of the g_z for the lowest two exchange doublets of complex **1-Dy**.

	1-Dy		
Exchange Doublets	*E*	Δ_t	g_z
1	0.000000000000	1.75×10^{-6}	0.000
	0.000001752381		
2	4.274845608914	6.35×10^{-7}	39.536
	4.274846244345		

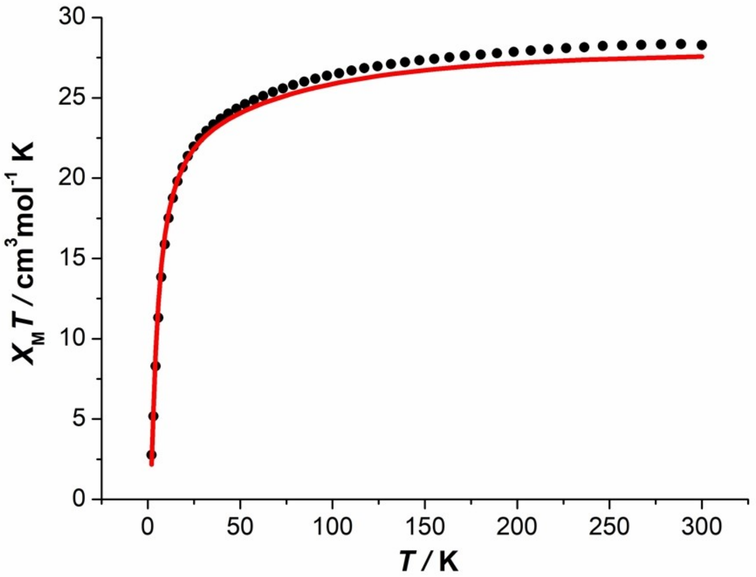

Fig. S30 Calculated (red solid line) and experimental (black circle dot) data of magnetic susceptibilities of **1-Dy**. The intermolecular interactions zJ' of **1-Dy** was fitted to –0.02 cm^{-1}.

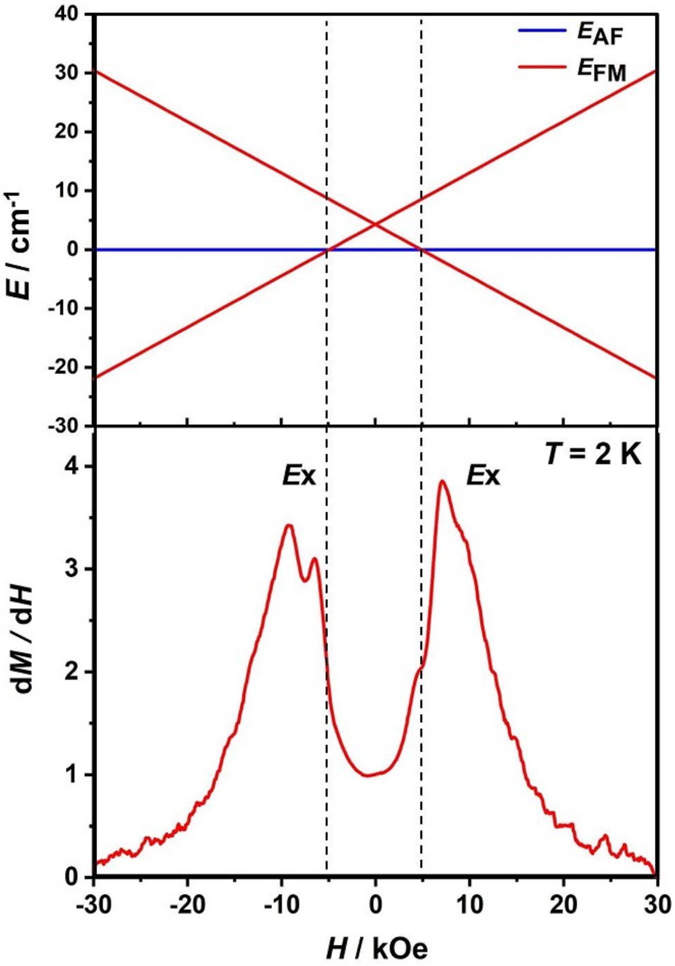

Fig. S31 Zeeman diagrams (top) and the first derivative of the hysteresis loops (bottom) for **1-Dy**.

References

1. O. V. Dolomanov, L. J. Bourhis, R. J. Gildea, J. A. K. Howard and H. Puschmann, Olex2: A complete structure solution, refinement and analysis program, *J. Appl. Crystallogr.*, 2009, **42**, 339-341.
2. G. M. Sheldrick, A short history of shelx, *Acta Crystallogr A*, 2008, **64**, 112-122.
3. G. Sheldrick, Crystal structure refinement with shelxl, *Acta Crystallographica Section C*, 2015, **71**, 3-8.
4. M. Liu, Y.-C. Chen, J. Zheng, X.-H. Peng, M.-L. Tong, A. Mansikkamäki and F.-S. Guo, Isolation and single-molecule magnetism of neutral rare-earth(III) sandwich complexes supported by compact aromatic rings, *Sci. China Chem.*, 2025, **68**, 2978-2986.
5. G. A. Bain and J. F. Berry, Diamagnetic corrections and pascal's constants, *J. Chem. Educ.*, 2008, **85**, 532.
6. I. Fdez. Galván, M. Vacher, A. Alavi, C. Angeli, F. Aquilante, J. Autschbach, J. J. Bao, S. I. Bokarev, N. A. Bogdanov, R. K. Carlson, L. F. Chibotaru, J. Creutzberg, N. Dattani, M. G. Delcey, S. S. Dong, A. Dreuw, L. Freitag, L. M. Frutos, L. Gagliardi, F. Gendron, A. Giussani, L. González, G. Grell, M. Guo, C. E. Hoyer, M. Johansson, S. Keller, S. Knecht, G. Kovačević, E. Källman, G. Li Manni, M. Lundberg, Y. Ma, S. Mai, J. P. Malhado, P. Å. Malmqvist, P. Marquetand, S. A. Mewes, J. Norell, M. Olivucci, M. Oppel, Q. M. Phung, K. Pierloot, F. Plasser, M. Reiher, A. M. Sand, I. Schapiro, P. Sharma, C. J. Stein, L. K. Sørensen, D. G. Truhlar, M. Ugandi, L. Ungur, A. Valentini, S. Vancoillie, V. Veryazov, O. Weser, T. A. Wesołowski, P.-O. Widmark, S. Wouters, A. Zech, J. P. Zobel and R. Lindh, Openmolcas: From source code to insight, *J. Chem. Theory Comput.*, 2019, **15**, 5925-5964.
7. P. Å. Malmqvist, B. O. Roos and B. Schimmelpfennig, The restricted active space (ras) state interaction approach with spin–orbit coupling, *Chem. Phys. Lett.*, 2002, **357**, 230-240.
8. B. A. Heß, C. M. Marian, U. Wahlgren and O. Gropen, A mean-field spin-orbit method applicable to correlated wavefunctions, *Chem. Phys. Lett.*, 1996, **251**, 365-371.
9. L. F. Chibotaru, L. Ungur and A. Soncini, The origin of nonmagnetic kramers doublets in the ground state of dysprosium triangles: Evidence for a toroidal magnetic moment, *Angew. Chem. Int. Ed.*, 2008, **47**, 4126-4129.
10. L. F. Chibotaru and L. Ungur, Ab initio calculation of anisotropic magnetic properties of complexes. I. Unique definition of pseudospin hamiltonians and their derivation, *J. Chem. Phys.*, 2012, **137**, 064112.
11. L. F. Chibotaru, L. Ungur, C. Aronica, H. Elmoll, G. Pilet and D. Luneau, Structure, magnetism, and theoretical study of a mixed-valence $Co^{II}_3Co^{III}_4$ heptanuclear wheel: Lack of smm behavior despite negative magnetic anisotropy, *J. Am. Chem. Soc.*, 2008, **130**, 12445-12455.
12. B. Yin and C.-C. Li, A method to predict both the relaxation time of quantum tunneling of magnetization and the effective barrier of magnetic reversal for a kramers single-ion magnet, *Phys. Chem. Chem. Phys.*, 2020, **22**, 9923-9933.
13. M. E. Lines, Orbital angular momentum in the theory of paramagnetic clusters, *J. Chem. Phys.*, 1971, **55**, 2977-2984.
14. K. C. Mondal, A. Sundt, Y. Lan, G. E. Kostakis, O. Waldmann, L. Ungur, L. F. Chibotaru, C. E. Anson and A. K. Powell, Coexistence of distinct single-ion and exchange-based mechanisms for blocking of magnetization in a $Co(II)_2$-Dy-$(III)_2$ single-molecule magnet, *Angew. Chem. Int. Ed.*, 2012, **51**, 7550-7554.
15. S. K. Langley, D. P. Wielechowski, V. Vieru, N. F. Chilton, B. Moubaraki, B. F. Abrahams, L. F. Chibotaru and K. S. Murray, A $\{Cr(III)_2Dy(III)_2\}$ single-molecule magnet: Enhancing the blocking temperature through 3d magnetic exchange, *Angew. Chem. Int. Ed.*, 2013, **52**, 12014-12019.